International Journal of Geosynthetics and Ground Engineering (2022) 8:70
https://doi.org/10.1007/s40891-022-00414-x

ORIGINAL PAPER

Physical and Computational Modelling of Geosynthetic-Reinforced Model Slopes in Shaking Table Tests

N. Srilatha[1] · **G. Madhavi Latha**[2]

Received: 2 June 2022 / Accepted: 23 October 2022 / Published online: 5 November 2022

Abstract

The effectiveness of tensile reinforcement in controlling the deformations of soil slopes under sinusoidal base shaking conditions is studied through model tests carried out on shaking table and the results are analyzed using computational modelling based on Newmark's rigid block analysis. The acceleration and frequency of shaking are varied in different model tests, simulating low and high frequency seismic events of different accelerations. To control the acceleration amplifications and displacements, slope models were reinforced using geogrids placed at different heights of the model. While unreinforced slopes showed higher seismic response at low-frequency high-acceleration motions, exhibiting a sudden flow slide type of failure, reinforced slopes showed very less deformations and stayed stable during all events. Slope deformations were computed using Newmark's rigid block analysis, considering the peak and residual yield accelerations of the model slopes. The deformations computed using modified Newmark's analysis are in good agreement with the measured deformations for unreinforced cases at all frequencies and for reinforced cases at lower frequencies. The analytical models overpredicted the seismic deformations of reinforced slopes at higher frequencies due to the possible alterations to interface shear mechanisms, leading to a significant difference in actual and computed yield accelerations.

Keywords Reinforced slope · Shaking table · Seismic response · Yield acceleration · Rigid block analysis

Introduction

The idea of making stable soil slopes by including layers of reinforcing elements is age-old but the research on improving these elements to suit contemporary construction scenarios is forever evolving. Reinforced soil slopes provide faster and cost-effective solutions for situations where the construction requires steeper slopes. Such slopes are typically used for embankments, dams, levees, flood protection systems, landslide rehabilitation, and landfills. Reinforced soil slopes have become important elements of many infrastructural projects worldwide, since they allow construction of very steep slopes, thus saving space and materials. The material, form, and structure of the reinforcing elements have undergone several changes over the past five decades. Geosynthetics, which are polymeric materials, are extensively being used for soil reinforcement because they are non-corrosive, cheaper, and easier to install, compared to metal strips. Geogrids and geotextiles are the most common forms of geosynthetics that are used for the construction of mechanically stabilized soil slopes.

The concept of improving the stability of soil slopes by the inclusion of reinforcing layers was well explained by earlier researchers [1, 2]. Studies revealed that the reinforcing layers cause reorientation of principal strain axes and reduce the tensile strains in the surrounding soil to a greater extent. Since the geosynthetic layers are extensible, they deform near the failure plane, thus generating peak tension in reinforcement at this point because of friction, resulting in highest shearing resistance along the failure plane. Construction of geosynthetic reinforced soil slopes has reached a level of excellence and many steep slopes are being constructed with confidence for supporting extremely high static and cyclic loads. As the demand for steeper slopes is increasing due to space constraints, interface shear strength of soil and

✉ N. Srilatha
srilathanbr@gmail.com

G. Madhavi Latha
madhavi@iisc.ac.in

[1] Department of Civil Engineering, MSRIT, Bangalore 560054, India

[2] Department of Civil Engineering, Indian Institute of Science, Bangalore 560012, India

geosynthetics is often a limiting factor for building steep slopes. Manufacturing of geosynthetics with texture and spikes has improved the soil–geosynthetic interface shear strength to the extent that very steep slopes are being constructed without much difficulty.

Any seismic event can induce instability in slopes because the induced vibrations can break the contacts among the soil grains. Also, vibrations impose additional driving forces on the soil slopes which trigger the failure of slopes whenever the driving forces exceed the shear strength of the soil. Soil slopes with reinforcement provide better resistance to these vibrations than the unreinforced slopes as reinforced slopes possess higher yield acceleration than unreinforced slopes. The additional horizontal seismic driving forces on the slope, which are the major reason for slope failures in seismic events, are opposed by the tensile forces developed in the reinforcement strips. After the 1994 Northridge earthquake of California of 6.7 magnitude, performance of numerous reinforced soil structures was documented by many researchers, including Bathurst and Cai [3], Sandri [4, 5]. Of those structures reported, the highest slope was of 24.5 m, which was built with geogrid reinforcement. Though the slope showed some signs of distress, it could withstand almost twice the acceleration value it was designed for [5]. Among the many factors that govern the seismic response of reinforced soil slopes, the important slope parameters are the physical and mechanical properties of the slope soil, stiffness and interface friction properties of the reinforcement and the slope geometry. Ground motion parameters, which include the amplitude and frequency of shaking, are also very important because they directly represent the intensity of shaking. Interestingly, increase in the amplitude or frequency need not increase the response of model in terms of deformations and acceleration amplifications. Similarly, gradation and particle size distribution of slope material will not give direct clues to the response of the slope to different intensities of shaking. The response of the model depends on the rheological properties of the slope material under imposed shaking conditions. Maximum response in the model can be the result of a certain combination of slope parameters and base shaking parameters, which are not too obvious to detect without controlled testing. This aspect forms the main motivating factor for the present study.

From the past three decades, many researchers have demonstrated the use of shaking table for modelling soil structures under base shaking conditions. Soil retaining walls, foundation beds, embankments, and slopes were successfully built and tested in shaking tables [6–14]. Shaking table studies have many advantages, which include the relatively large sized models that can be built and tested, the benefit of using embedded instrumentation in models without any significant effect on their response, and plane strain conditions in the models that closely coincide with the actual field conditions [15]. There are also some limitations associated with the shaking table model testing. Wood et al. [16] emphasized the importance of scaling laws in physical modeling and discussed their application to shaking table modelling. As the studies on shaking table are 1-*g* model tests unlike centrifuge tests, the model test results cannot be extrapolated directly to the field conditions. Similitude laws proposed by many researchers [17–20] correlate the results of shaking table tests to field conditions. Among these, the similitude laws derived by Iai [18] based on the equation of motion in 1-*g* gravitational field, are very well accepted by the geotechnical researchers.

Most of the shaking table model studies available on the dynamic testing of soil structures are related to the retaining walls. Studies related to the response of soil slopes under cyclic loading conditions are very limited [21]. Fahliani et al. [22] showed the behavior of a strip footing resting on unreinforced and geocell-reinforced sand slopes with change in the dimensions of the geocell layer, setback of the footing and the slope angle. The study carried out by Matsuo et al. [23] on a 1 m high, 1H:5 V reinforced slope with discrete panel facing subjected to seismic accelerations between 0.1 and 0.44 *g* showed failure and pullout of the lower layers of reinforcement. Significant number of studies are also available on the centrifuge testing of the reinforced soil slopes [24–29].

Analytical models that can accurately predict the slope deformations in seismic conditions can be very beneficial. A model which is proved to be successful for laboratory model tests can be extended to predict the deformations of slopes in field, after applying appropriate scaling adjustments. The rigid block analysis, which is conceptualized by Newmark [30] based on limit equilibrium approach, is a very simple and useful method to compute the permanent deformations in a slope subjected to seismic vibrations. However, this method suffers from the limitations of the limit equilibrium approach and assumes that the slope does not deform before the yield acceleration is reached. The pseudo-static rigid block analysis of Newmark was modified into pseudo-dynamic analysis by Steedman and Zeng [31], to compute the slope deformations more accurately. While the Newmark's method of displacement estimation is based on a single parameter called yield acceleration, Steedman and Zeng's method includes the combined effects of time, phase difference, and yield acceleration, to calculate the slope displacements. Later Zeng and Steedman [32] verified this analysis for predicting the deformations in model walls subjected to seismic shaking in a centrifuge. A few more pseudo-dynamic analytical models were proposed by other researchers [33, 34]. These displacement models were tested by many other researchers for computing model slope deformations and compare them with the measured values. Such comparison was done by Wartman et al. [35] for clay

slopes tested in shaking table. For this case, the rigid block model was able to effectively predict the displacements for the model tests that experienced huge deformations. Yield accelerations were computed using peak and residual friction angles separately, computing the range of displacements possible for the slope. Unlike earlier studies of Matasovic et al. [36] where critical acceleration was computed to be degrading from a higher value calculated using peak friction angle to a lower value calculated using residual friction angle at threshold displacement. Ichii and Ohmi [37] studied the behavior of model slopes built with cohesionless materials under large seismic shaking through shaking table tests. Results from this study showed that slope angles after failure in static inclination tests were far smaller than the threshold slope angle, which can be calculated using internal friction angle. It was suggested that displacements evaluated by the Newmark's method can be a good index for damage level evaluation for slopes.

Particle image velocimetry (PIV) technique is employed by some researchers to trace the displacements in models during dynamic shaking. One such study was reported by Wang and Lin [38] for sand slopes constructed and tested on a shaking table. This study demonstrated that the laws of similitude will not be valid once failure is initiated in the slope. A similar argument was earlier made by Kawai [39] while investigating the use of scaled models in geotechnical engineering through various physical modelling problems involving a sea wall, an underground structure, and a slope. While comparing the stress–strain behavior of soils assumed in similitude laws and realistic stress–strain behavior, it was illustrated that the similitude laws are valid only for low to medium strain ranges. Numerical studies carried out by Zhang et al. [40] to understand the effects of topography on acceleration amplifications revealed that the crest of the slope need not always experience peak amplification and the amplifications are mainly governed by the geometry of the slope in relation with the wavelength of shaking and material heterogeneity. Most recent studies by Xu et al. [13] on reinforced retaining walls subjected to stepped-amplitude harmonic base excitation also verified the accuracy of pseudo-static methods for the computation of acceleration amplifications and deformations in shaking table models.

As stated earlier, shaking table model studies in literature are dominated by retaining wall studies. The response of soil slopes to seismic conditions is mainly studied through analytical and numerical models. Hence, many important behavioral aspects of soil slopes to base shaking conditions remained only theoretical. The present study is mainly focused on examining the response of sand slopes to sinusoidal shaking and analyzing the effects of shaking frequency and acceleration through physical model studies. Beneficial effects of tensile reinforcement elements in controlling the acceleration amplifications and slope deformations are also investigated. To complement the physical model studies, slope deformations are analytically computed using Newmark's sliding block method and compared with the model test measurements. The applicability of analytical slope deformation computations for unreinforced and reinforced model slopes is discussed, based on these comparisons.

Experimental Setup, Materials, and Instruments Used

Shaking Table

Physical model tests in this study were carried out on a shaking table, which can produce horizontal base shaking with controlled frequency (1 to 50 Hz) and acceleration amplitude (0.1 to 2 g). The system can support testing of structures weighing up to 1000 kg. A square table of 1 m sides provides the base for mounting the structures. In this study, a laminar box was used to build the slopes, to minimize the boundary effects during shaking. The laminar box is made up of aluminum panels stacked with rollers in between, to allow frictionless movement of the individual panels. The box is 800 mm deep, having inner plan dimensions of 1 m length and 500 mm width. The laminar box is rigidly fixed to the top of the shaking table, with its length placed in the direction of shaking. This arrangement ensures plane strain conditions within the slope models. Krishna and Latha [41] demonstrated the effectiveness of this laminar box in reducing the boundary effects in shaking table model studies, by comparing the performances of identical models built in a rigid box and the laminar box.

Soil

Slope models were built using local soil. Sieve analysis showed that the soil is uniformly graded sand with particle sizes falling in the range of medium sand, as shown in Fig. 1. Grain size fractions and other physical properties of the sand are listed in Table 1.

Reinforcement

Geogrids were used as reinforcing sheets in model slopes. These geogrids are biaxial, with 35 mm square apertures. Multi-rib tension tests were conducted on multiple geogrid specimens of size covering five ribs in width and three ribs in height as per ASTM: D6637/D6637M [42] to obtain average tensile properties of the geogrid, as listed in Table 2. Physical dimensions and mass density of the geogrids are also listed in Table 2. The load elongation response of geogrid in the multi-rib tension test is shown in Fig. 2.

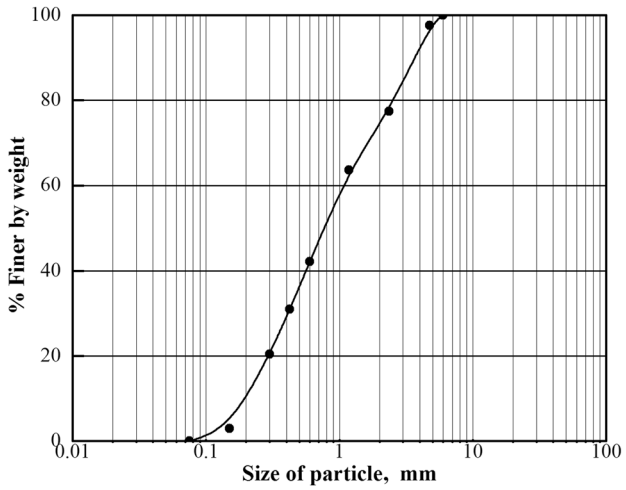

Fig. 1 Grain size distribution of the sand

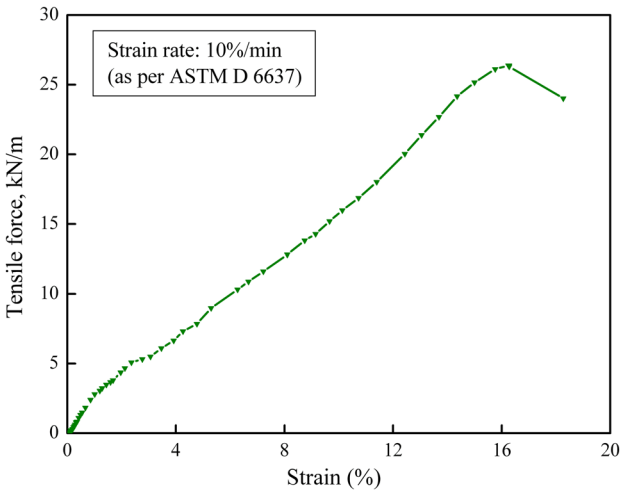

Fig. 2 Load-elongation response of geogrid in the multi-rib tension test

Table 1 Grain size fractions and other physical properties of the sand

Property	Value
Specific gravity	2.65
% Gravel size fraction	2.5
% Sand size fraction	97
% (Silt + Clay) size fraction	0.5
Effective size of particle, D_{10} (mm)	0.22
Coefficient of uniformity (C_u)	5
Coefficient of curvature (C_c)	0.74
Maximum void ratio (e_{max})	0.733
Minimum void ratio (e_{min})	0.444
Maximum dry unit weight, γ_{dmax} (kN/m^3)	18.1
Minimum dry unit weight, γ_{dmin} (kN/m^3)	15.0
Classification	Poorly graded sand (SP)

Table 2 Physical dimensions and tensile properties of the geogrid

Property	Value
Ultimate tensile strength (kN/m)	26
Failure strain (%)	16.50
Aperture size (mm)	35 × 35
Aperture shape	Square
Secant modulus at 5% strain (kN/m)	167
Mass per unit area (kg/m^2)	0.22

Instrumentation

Analog output type accelerometers of BiSS make ADXL311 model were used to instrument the slope models. These accelerometers have a sensing range of ± 2 g in both the horizontal directions, within the bandwidth of 1–2 kHz. Models were also instrumented with Banner make U-GAGE S18U displacement sensors. These sensors work on non-contact sensing technology and measure the displacements based on the reflection time of ultrasonic waves emitted by the sensors. The auto-teach function of these sensors automatically estimates the distance between the sensor and the moving object and hence the error is minimized. The response time is as low as 5 ms. The automatic data acquisition system of the shaking table has a controller, to which the sensors are connected and controlled.

Construction of the Models and Testing Procedure

All model slopes have identical dimensions of 600 mm height, 850 mm length, and 500 mm width. The crest width was 250 mm, and the slope angle was 45°. The length of the model is in line with the shaking direction. Initially, the geometry of the slope model is marked on the base and walls of the laminar box. A vertical wooden panel was erected at the toe of the slope, to the full height of the laminar box and supported using concrete blocks on the other side. Inside the rectangular space of 850 mm length, 500 mm width bounded by the sidewalls of the laminar box and the wooden panel, sand is filled and compacted in equal lifts of 200 mm thickness. Water content in the sand was maintained at 10–10.5%. A 5 kg mass lifted and dropped over a 150 mm square steel plate from a height of 450 mm through a guide-rod arrangement was used to compact the soil layers. Many trials were carried out to arrive at the number of compacting blows required for each lift to achieve a final thickness of 200 mm at the target unit weight of 17–17.5 kN/m^3 in model slopes. Unit weight of soil in model slopes was verified from cores

taken at random locations at each depth. Coring was done by carefully pushing the split former into the slope model and carefully carving the slope to remove the sampler after it is pushed to required depth. Suction was applied while the sample is mounted on the pedestal of triaxial cell, and the split former was carefully removed while the vacuum is applied. This ensured extraction of relatively undisturbed samples. However, 100% undisturbed sampling is impossible in sands. But the cored samples represent the model state better than the remolded samples. Similarly, water content was checked by oven drying these samples. Variation in unit weight of soil and its water content across different samples in all model tests was within 5%. Shear strength properties of soil at this unit weight and water content, representing the state in slope models were determined from unconsolidated undrained (UU) triaxial tests as per IS 2720 (Part 11) [43]. The cohesion and peak friction angle of the sand samples were determined as 2.4 kPa and 38º, respectively, in UU test.

Schematic plan and elevation of a typical reinforced slope instrumented with sensors are shown in Fig. 3. Accelerometer A0 fixed at the center of the shaking table base measures the acceleration input to the slope model. A1 at 170 mm, A2 at 370 mm, and A3 at 570 mm from the base of the slope, all at 50 mm away from the slope face, embedded into the sand, measure acceleration amplifications at different heights of the model. Since the displacement sensors are non-contact type, they were rigidly fixed to thick wooden posts fitted to the steel bracket placed in front of the slope face. Their heights were fixed as 200 mm (U1), 350 mm (U2), and 500 mm (U3) from the base, to measure deformations at different heights. Calibration of the displacement sensors under shaking conditions was carried out before the start of each model test, when the laminar box was empty. The natural frequency of the slope model was determined as 8.3 Hz in sine weep test.

In reinforced slope models, at pre-determined height, geogrid layers were placed to the full width of the slope, up to 50 mm from the face of the slope. Though this configuration is uneconomical because reinforcement length beyond the anchor length does not contribute to the stability of the slope, it was chosen to keep the reinforcement configuration simple and uniform in all the tests. Test results are not affected by this extra length of reinforcement because the reinforcement length needed beyond the failure surface for anchorage is available in all the tests and the extra length does not have any effect on the performance of the slope [44]. Once the compaction of soil to the required height of the slope was reached, the compacted soil was carefully trimmed as per the slope geometry of slope marked on the side walls of the laminar box, using a hand shovel. Figure 4 shows the slope marking, sand filling, and geogrid placement inside the laminar box (Fig. 4a) and the final slope (Fig. 4b).

A total of fourteen model tests were carried out on sand slopes, eight of them on unreinforced slope models and the other six on the geogrid-reinforced slope models. Table 3 gives the test parameters used in different model tests. Test code given for each model tests denotes the input parameters used in that specific test, including the model type (unreinforced or reinforced), frequency of base motion, and acceleration amplitude. The first letter of the test code indicates whether the test is done on an unreinforced (U) or a reinforced (R) model. For reinforced model slopes, the letter symbol R is followed by the number of reinforcing layers. Four different frequencies were used in the model tests, which are represented in the test code with F1 (1 Hz

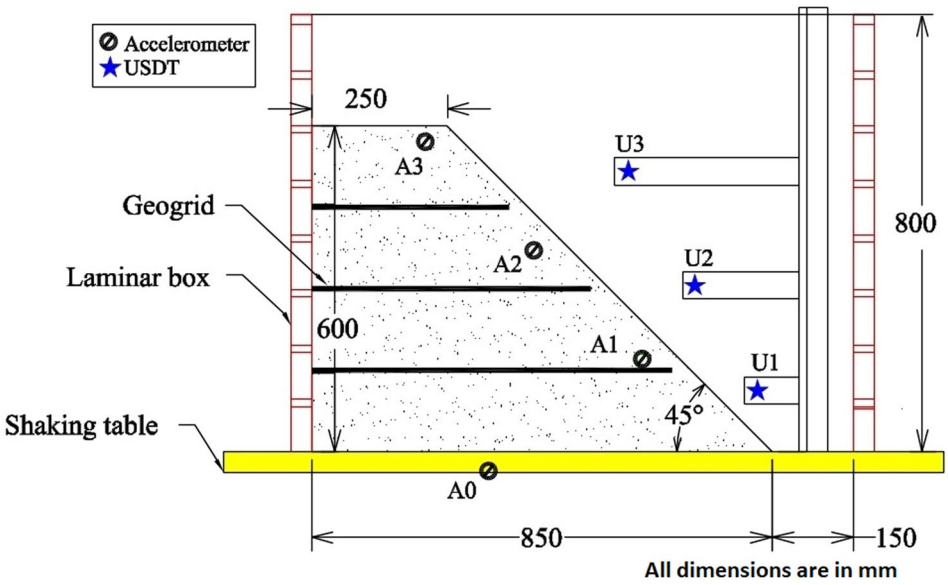

Fig. 3 Schematic representation of a typical reinforced slope instrumented with sensors

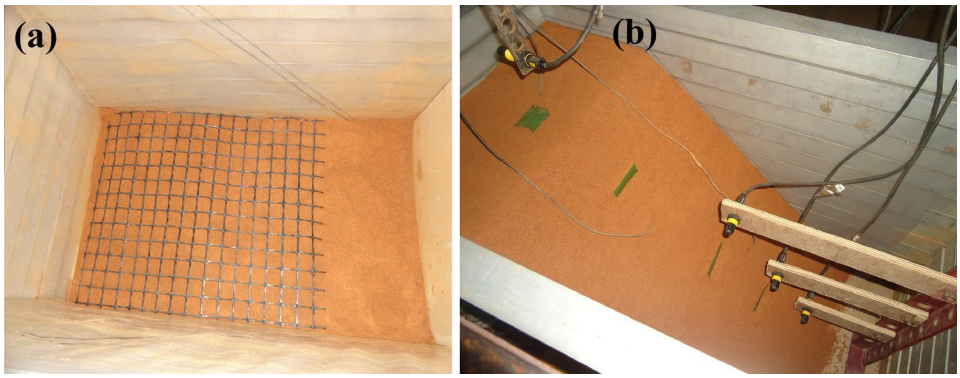

Fig. 4 Photographs of model construction **a** slope marking, sand filling, and geogrid placement inside the laminar box and **b** final slope

Table 3 Test parameters used in different model tests

S. No	Test code	Reinforcement	Frequency (Hz)	Acceleration (*g*)
1	UF1A3	UR	1	0.3
2	UF1A3 (R)	UR	1	0.3
3	UF2A3	UR	2	0.3
4	UF2A3 (R)	UR	2	0.3
5	UF5A3	UR	5	0.3
6	UF7A3	UR	7	0.3
7	UF2A1	UR	2	0.1
8	UF2A2	UR	2	0.2
9	R1F2A3	1 layer	2	0.3
10	R2F2A3	2 layer	2	0.3
11	R3F2A3	3 layer	2	0.3
12	R1F7A3	1 layer	7	0.3
13	R2F7A3	2 layer	7	0.3
14	R3F7A3	3 layer	7	0.3

frequency), F2 (2 Hz frequency), F5 (5 Hz frequency), and F7 (7 Hz frequency). Three different acceleration amplitudes were used in the model tests, which are represented by A1 (amplitude of 0.1 *g*), A2 (amplitude of 0.2 *g*), and A3 (amplitude of 0.3 *g*) in the test code. For example, test code UF1A3 represents the model test on an unreinforced model soil slope carried out at 1 Hz base shaking frequency and 0.3 g acceleration amplitude. Similarly, test code R1F2A3 represents the model test on a soil slope reinforced with a single layer of geogrid carried out at a frequency of 2 Hz and acceleration amplitude of 0.3 *g*.

Results and Discussion

For all model tests, acceleration amplitudes at different locations were recorded using the accelerometers A0 fitted to the shaking table and A1, A2, and A3 embedded inside the slope, as shown in Fig. 3. Deformations of the model slope were measured using the sensors U1, U2, and U3, mounted in front of the slope. The accelerometer A0 always measures the acceleration of the table, without any amplification and hence is a check for the input acceleration supplied to the model. To ensure that the displacement measurements are accurate, trial tests were carried out on empty table with the deformations of a vertical steel post measured by shifting it to different locations along the line of measurement and comparing the recorded displacements with the physical measurements of these movements. These trial tests confirmed that the difference in these measurements is less than 0.5 mm.

Root mean square acceleration (RMSA) amplification factors are used to simplify the presentation of acceleration response at different elevations of the slopes. These factors are calculated using the root mean square (RMS) method applied to the acceleration time history for each accelerometer device. The RMSA value was calculated using the following equation given by Kramer [45].

$$RMS = \left[\frac{1}{t_d} \int_0^{t_d} a(t)^2 dt \right]^{\frac{1}{2}} \quad (1)$$

where $a(t)$ is the acceleration time history, t_d is the duration of the acceleration record, and dt is time interval of the acceleration record. This integral is evaluated using the integral function in spreadsheet program Excel, using the acceleration time history recorded during the test. The ratio of soil response acceleration value to the base motion corresponding value (recorded on A0) is termed as RMSA amplification factor.

Performance of Unreinforced Sand Slopes

Performance at Different Frequencies

Repeatability of test results is a big challenge in physical modeling, which requires that the models must be identical in their geometry, composition, and properties, the shaking

table should be resilient to transmit the exact input ground motion parameters every time, and the sensors should be accurate to record the correct output parameters. Many of the model tests were repeated initially, to confirm the results. Typical acceleration time histories at different locations for the test UF2A3 are shown in Fig. 5. Acceleration time histories of the repeated model test of UF2A3, which is represented with test code UF2A3 (*R*) are shown in Fig. 6. Comparison of RMSA amplification factors and horizontal deformations at identical locations of two different models UF1A3 and UF2A3 with their repeated models UF1A3 (*R*) and UF2A3 (*R*) is shown in Fig. 7. These plots show close

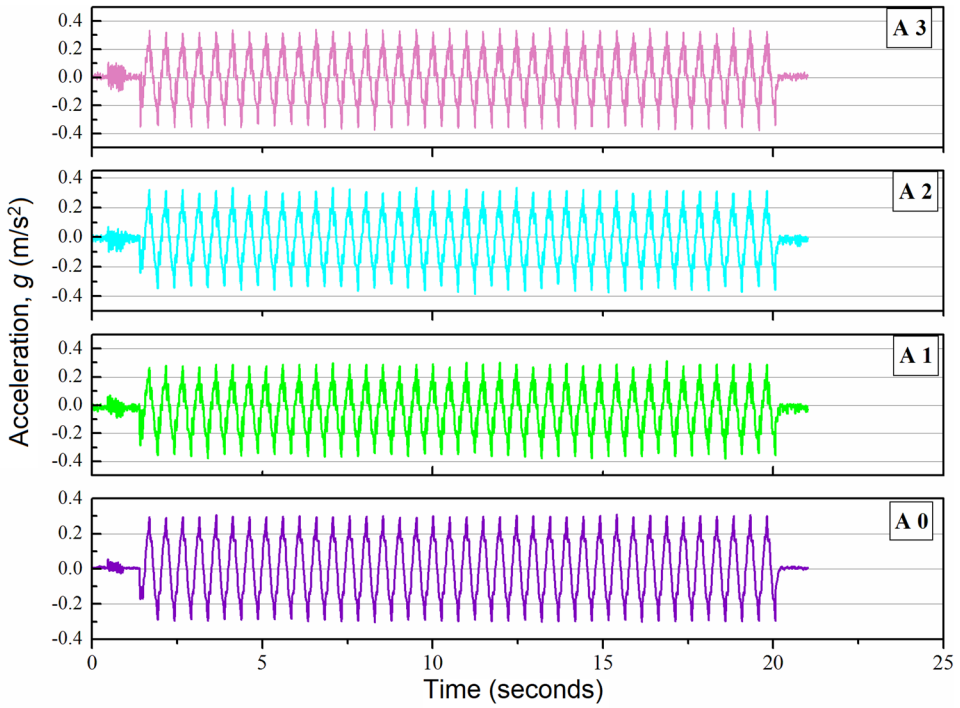

Fig. 5 Typical acceleration time histories at different locations for the test UF2A3

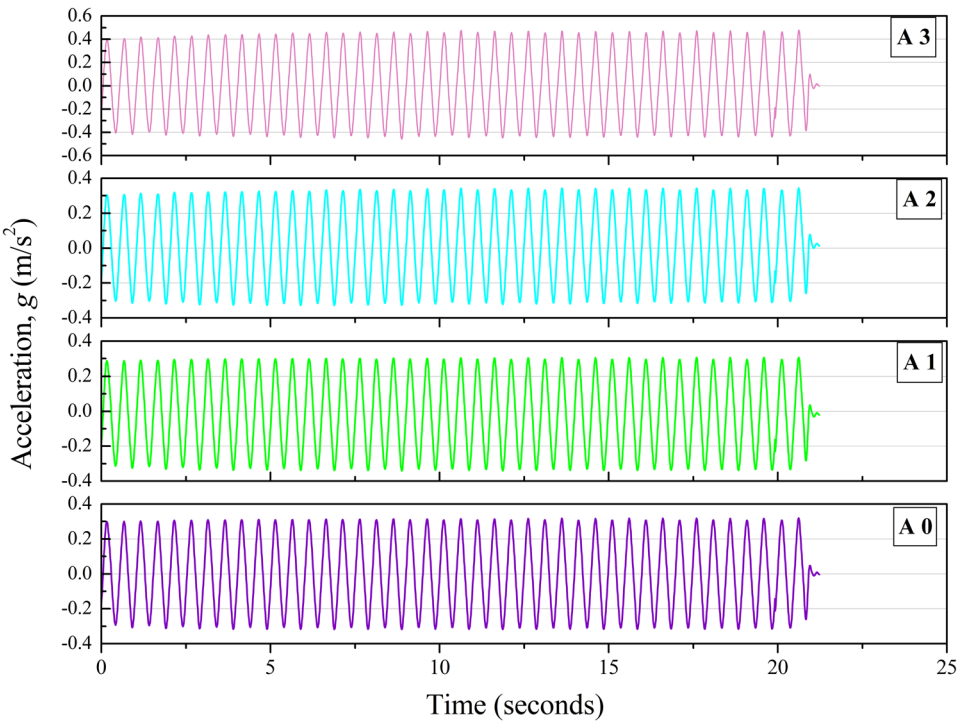

Fig. 6 Acceleration time histories of the repeated model test of UF2A3, which is represented with test code UF2A3 (R)

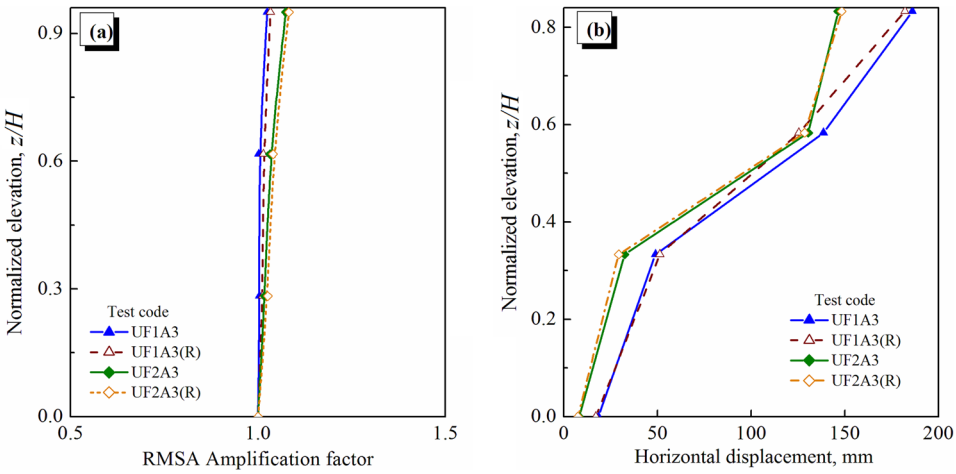

Fig. 7 Comparison of the performance of two different models UF1A3 and UF2A3 with their repeated models UF1A3(R) and UF2A3 (R) **a** RMSA amplification factors and **b** horizontal displacements

agreement between the horizontal displacements and the acceleration amplifications in repeated tests.

Results showed that the acceleration amplification factors are slightly higher at the slope crest in all the tests. A small amount of base sliding was observed when the models were tested at low frequencies. The sliding displacements were 8.2 mm and 18.4 mm, measured in tests carried out at frequencies of 2 Hz and 1 Hz, respectively, as seen in Fig. 7b. Bathurst et al. [7] and Lo Grasso et al. [46] also observed higher acceleration amplifications at higher elevations. The higher acceleration amplification at the slope crest could be due to the geometry of the slope. In general, topography has significant influence on acceleration amplifications, revealed by many field measurements during seismic events, including the 1994 Northridge, California, earthquake, in which a peak horizontal acceleration of 1.58 was recorded on a ridge near the Pacoima dam while the peak horizontal acceleration recorded in surrounding flat areas was below 0.5 *g*. The effects of topography on acceleration amplifications were demonstrated by Brennan and Madabhushi [27] through centrifuge model tests on slopes. These tests revealed that seismic shaking amplifies the accelerations to their maximum at the crest of the slope and the extents affected by topography have greater extents horizontally than vertically. It was also observed that these effects are more beyond the natural frequency of the soil column. Horizontal displacements were also observed to be increasing with the elevation. The acceleration amplification factors and displacements given in all the plots correspond to the state at the end of 40 cycles of sinusoidal motion. Elevation is normalized with respect to height of the slope in all the plots.

A set of model tests was carried out to understand the response of the unreinforced sand slopes at different frequencies of base shaking. Figure 8a shows the acceleration response of unreinforced model sand slope to a base acceleration of 0.3 *g* and different frequencies 1, 2, 5, and 7 Hz (UF1A3, UF2A3, UF5A3, and UF7A3). With the increase in shaking frequency, acceleration amplification factors are increased, with highest model response observed at a frequency of 7 Hz. The computed maximum RMSA amplification factors recorded by A3 placed close to crest were 1.02, 1.07, 1.25, and 2.13 for frequencies of 1, 2, 5, and 7 Hz,

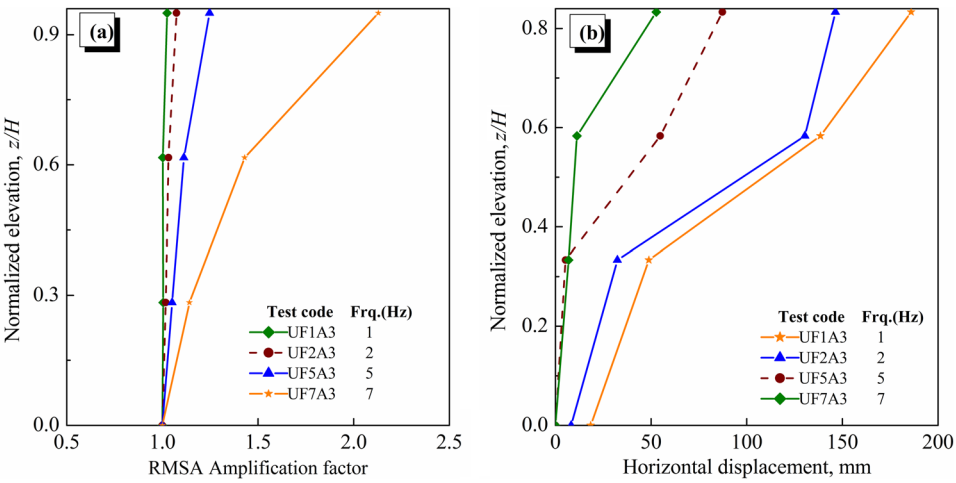

Fig. 8 Performance of unreinforced model slopes at four different frequencies **a** RMSA amplification factors and **b** horizontal displacements

respectively. Figure 8b provides the variation of horizontal displacements of unreinforced model slopes subjected to different frequencies of shaking. This plot indicates that slope displacements decreased with the increase in shaking frequency. Maximum displacements of 185.97 mm, 146.35 mm, 87.25 mm, and 52.68 mm were observed for 1 Hz, 2 Hz, 5 Hz, and 7 Hz frequencies, respectively. A similar trend of increasing displacements with a decrease in frequency was also observed at lower elevations of the model slopes. While sliding displacement of base was observed in slope models in tests at low frequencies of 1 Hz and 2 Hz as mentioned earlier, this base sliding was completely absent at higher frequencies of 5 Hz and 7 Hz, as seen from Fig. 8b. To confirm this behavior, most of these tests were repeated and the results from repeated tests showed close match, confirming that the model behavior is consistent. Many earlier researchers have suggested that the response of accelerations and displacements to frequency variation correspond to different regions of vibration spectrum. At low frequencies (up to 2 Hz), displacements are higher, and accelerations are smaller, while at higher frequencies, displacements are smaller and accelerations are higher [47]. Recently, Wood [48] demonstrated the effects of frequency on accelerations and displacement of a system vibrating under the influence of sinusoidal cyclic loading and showed that the increasing frequency increases acceleration amplitude and reduces displacement amplitude. Since higher frequencies correspond to shorter period, the vibrating mass has less time for movement and hence undergoes lesser displacements. On the other hand, since the vibrating mass has to achieve the specific peak velocity within this shorter time, the acceleration must increase. Results from the shaking table studies on model slopes reported in this paper support these findings.

Figure 9 shows photographs of model slope before shaking (Fig. 9a) and at the end of 40 cycles of base shaking at frequencies of 1 Hz (Fig. 9b), 2 Hz (Fig. 9c), and 7 Hz (Fig. 9d), respectively. Shaking acceleration was 0.3 *g* in all these model tests. From the comparison of photographs pertaining to tests at different frequencies shown in Fig. 9, it can be observed that the model slope has shown extensive cracking, particularly at lower frequencies. Amount of cracking and displacements increased from 2 Hz frequency to 1 Hz frequency, which is evident when Fig. 9b, c are compared. A maximum displacement of 146 mm was observed when the shaking frequency was 2 Hz and it increased to 186 mm at a frequency of 1 Hz. From the results of this study, it is clear that slopes built with coarse-grained soils exhibit high response at low frequencies. Since cohesive forces are absent in sands, particles get separated easily under shaking and low-frequency high-amplitude motions trigger higher seismicity, which helps in the quick propagation of cracks through the slope, thus displaying higher deformations. Local site effects on seismicity were explained by several earlier researchers [45]. At higher frequencies, slopes made of coarse-grained soils do not have enough time between cycles for the development of cracks. At higher frequencies, attenuation of seismic energy plays predominant role in sands, which resulted in low response [49]. Response of

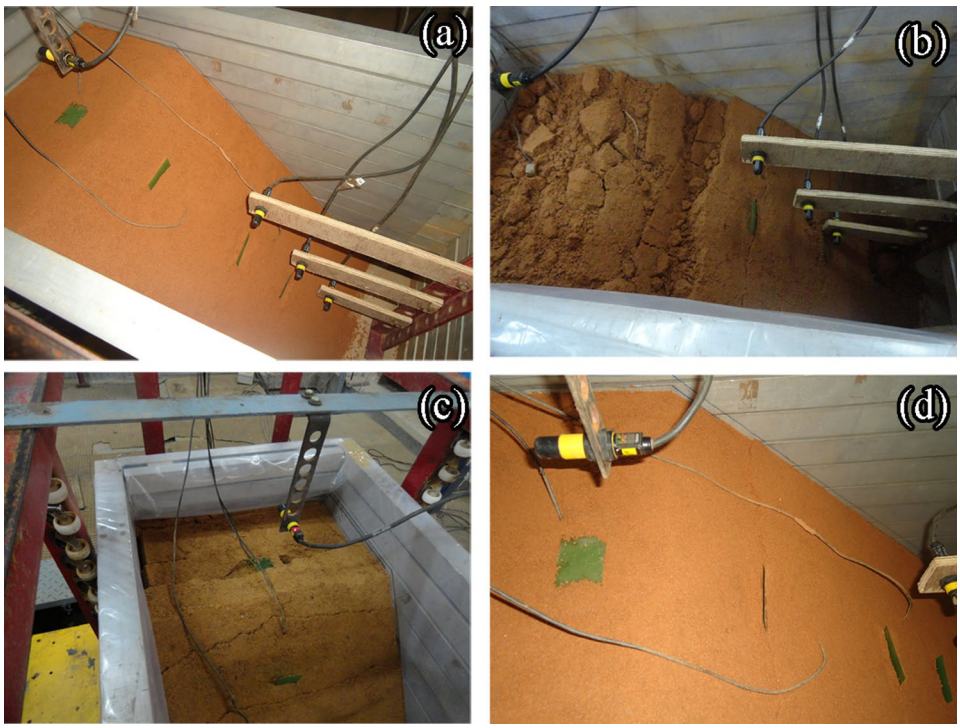

Fig. 9 Photographs of model slopes **a** before shaking and at the end of 40 cycles of base shaking at different frequencies, **b** 1 Hz, **c** 2 Hz and **d** 7 Hz

slope to the incoming ground motion can be totally contrasting with the change in slope material. Absence of fines in soil led to the increase in pore connectivity in slopes and the pores got disconnected easily at lower frequencies, leading to higher slope deformations. At higher frequencies, increased damping and attenuation of seismic energy in sands reduced the deformations of the slopes. Experiments presented in this section clearly demonstrated this fact and emphasized the need for site and material specific design of slopes for seismic conditions.

Performance at Different Accelerations

Performance of unreinforced model slope to shaking at three different accelerations, 0.1 *g*, 0.2 *g*, and 0.3 *g* is shown in Fig. 10. Frequency of shaking was 2 Hz in these model tests. Figure 10a shows the acceleration amplification response of unreinforced slopes made of sand (UF2A1, UF2A2, and UF2A3). Results showed that the acceleration amplifications in the model are not significantly different for different base acceleration conditions. The computed maximum RMSA amplification factors recorded by A3 placed close to the crest are 1.01, 1.02, and 1.07 for base accelerations 0.1 g, 0.2 *g*, and 0.3 *g*, respectively. The computed maximum RMSA amplification factors for the unreinforced slope are 1.01, 1.02, and 1.07 for base accelerations 0.1 g, 0.2 g, and 0.3 g, respectively. This variation is not much significant in case of small-scale models. However, in case of field slopes, the earthquake force, which is obtained by multiplying the acceleration with the mass of the slope, will be quite high at higher accelerations, as the amplification factor 1.07 leads to significantly higher earthquake force compared to the factor 1.01. The corresponding RMSA amplification factors at lower elevation recorded by A1 are1.00, 1.00, and 1.02, respectively. Figure 10b presents the displacement response of the unreinforced model slopes. The response indicates that there was a sudden increase in the displacements for the model test with base acceleration of 0.3 *g*, depicting a catastrophic failure, involving sudden sliding of the soil mass. Visual observations reinforced this behavior. Photograph of failed slope for this case is shown in Fig. 9b, which clearly indicated a landslide mass behavioral trend. The measured maximum displacement values at a normalized height of 0.95 were 3.34 mm, 4.66 mm, and 146.35 mm, respectively, for tests with base accelerations of 0.1 *g*, 0.2 *g*, and 0.3 *g*. At lower accelerations, the model slope did not show significant displacements since the forces that are driving the slope movement are resisted by the shear strength of the slope. The sudden increase in slope displacement with the increase in base motion from 0.2 to 0.3 *g* can be attributed to the increased driving forces due to increased shaking accelerations, which overcome the resisting forces and cause a flow type sliding failure in the slope. Analytical computations of the slope displacements and comparisons with the measured displacements are presented in subsequent sections. It is observed that, at a frequency of 1 Hz, the measured vertical settlement of the slope is in the order of 10–100 mm from the crest of the slope. Failure patterns observed in Fig. 9c showed several cracks on the slope, implying brittle behavior of slope mass, associated with subsequent dry debris slide, typical to flow slides in partially saturated sands [50]. This type of flow slides can be extremely dangerous in field, as the flowing land mass can be mobile and can move rapidly over gentle slopes, causing significant loss of life and damage to infrastructure in the vicinity. Hence, it is very important that the existing natural sandy slopes close to human habitat and infrastructure establishments in areas of high seismicity be stabilized using ground improvement techniques such as reinforcement, soil nailing, surface protection, and slope modification. Beneficial effects of soil reinforcement for slopes subjected to such severe earthquake conditions are investigated in subsequent sections.

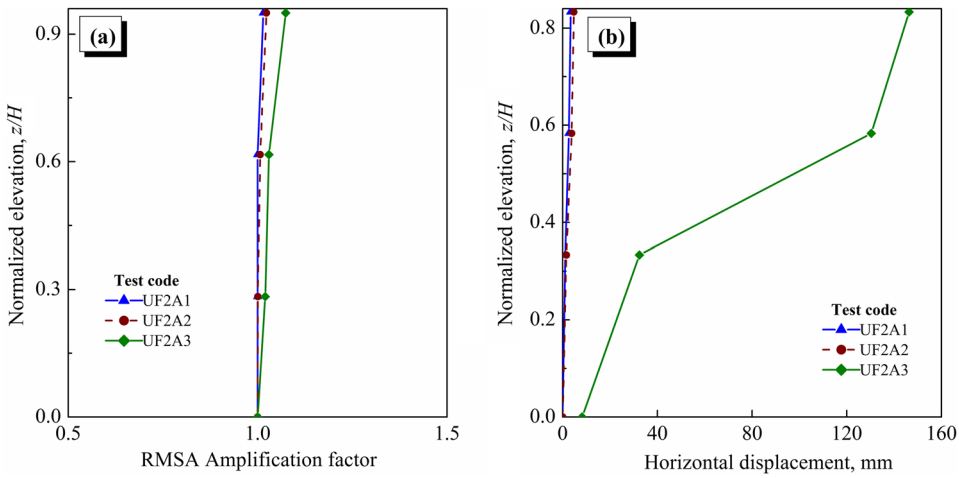

Fig. 10 Performance of unreinforced model slopes at three different accelerations **a** RMSA amplification factors and **b** horizontal displacements

Performance of Reinforced Sand Slopes

The static factor of safety for the unreinforced model slope is calculated as 1.075 using the limit equilibrium approach. Under earthquake conditions, this factor falls below 1.0, causing slope failure. Reinforcing the slopes using geosynthetics provides stability to slope under such conditions. To investigate this aspect, the model slope was reinforced with geogrid layers. The number of geogrid layers was 1, 2, and 3 in different tests, as explained in construction of models and testing procedure section. Performance of unreinforced and reinforced soil slopes subjected to identical shaking conditions are compared to understand the positive effects of geogrid reinforcement in reducing the acceleration amplifications and deformations of the slope.

Performance of unreinforced and different geogrid-reinforced slopes in terms of acceleration amplifications are compared in Fig. 11. Figure 11a shows the acceleration response of unreinforced and reinforced slopes subjected to 2 Hz frequency and base motion of 0.3 *g*. From Fig. 11, it is clear that the acceleration response of reinforced slopes is similar to that of unreinforced slope made of sand, with slight amplification observed at the crest of slope. No de-amplification was observed even in case of the heavily reinforced slope, indicating that the inclusion of reinforcement did not significantly increase the nonlinearity of soil behavior. However, when the frequency of shaking was increased to 7 Hz, the effect of reinforcement on acceleration amplification has become evident, as shown in Fig. 11b. All reinforced model slopes have displayed decrease in RMSA amplification factors compared to unreinforced model slope and the decrease in RMSA amplification factors is directly proportional to the increase in the reinforcement quantity. When the quantity of reinforcement is increased to three layers of geogrid, acceleration amplifications were brought down by more than 30%. The reason for this behavior is that the interfacial friction between sand and reinforcement increases with increase in frequency and with the increase in quantity of reinforcement. Through shaking table tests carried out on soil slopes reinforced with triaxial geogrid–waste tire composite, Lihua et al. [51] showed that the decrease in acceleration amplification factors with the inclusion of reinforcement in sandy slopes is 30–37.5%, which is similar to the observations made in the present study. Huang et al. [52] demonstrated that when the interface friction angle of the reinforcement was too low, reinforcement has negligible effect on the seismic stability of reinforced slopes. Increase in reinforcement layers improves the interfacial friction multifold, which effectively resists the acceleration amplifications of the slope models.

Figure 12 shows the horizontal displacements in unreinforced and reinforced model slopes. As observed from Fig. 12a, at a frequency of 2 Hz, the unreinforced slope showed a very high deformation of 146.35 mm at a normalized height of 0.95 and with the inclusion of one, two, and three layers of geogrid, the deformations reduced to 88.81 mm, 30.57 mm and 16.33 mm, respectively. Figure 12b shows the horizontal displacements in unreinforced and reinforced model slopes tested at 7 Hz frequency. At 7 Hz frequency, model slope deformed to a maximum extent of 52.68 mm and the deformation reduced to 9.01 mm, 6.74 mm, and 4.71 mm, respectively, for one-, two-, and three-layer geogrid-reinforced slopes. Maximum reduction in horizontal deformations was about 88%. Huge deformations were experienced by the unreinforced model slopes and these deformations were controlled effectively by including the reinforcement layers. Figure 12 shows that the difference in displacement response between the two-layer and three-layer reinforced soil slopes is not much significant, considering that the increase in the quantity of reinforcement is more than 30%. Reinforcement effect is maximum for the first layer, and it started reducing drastically after that. For the present case, two-layer reinforcement can be considered as reinforcement saturation. The stability of

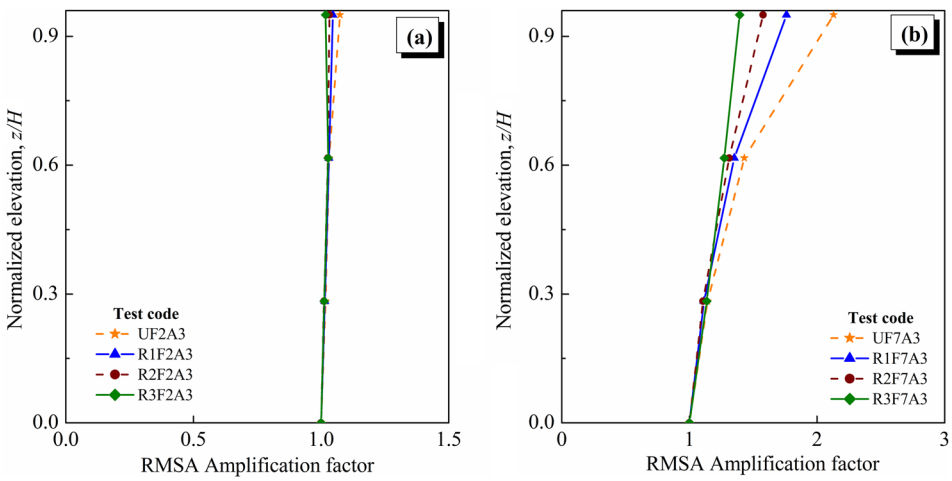

Fig. 11 Acceleration response of unreinforced and different geogrid-reinforced slopes at different frequencies **a** 2 Hz and **b** 7 Hz

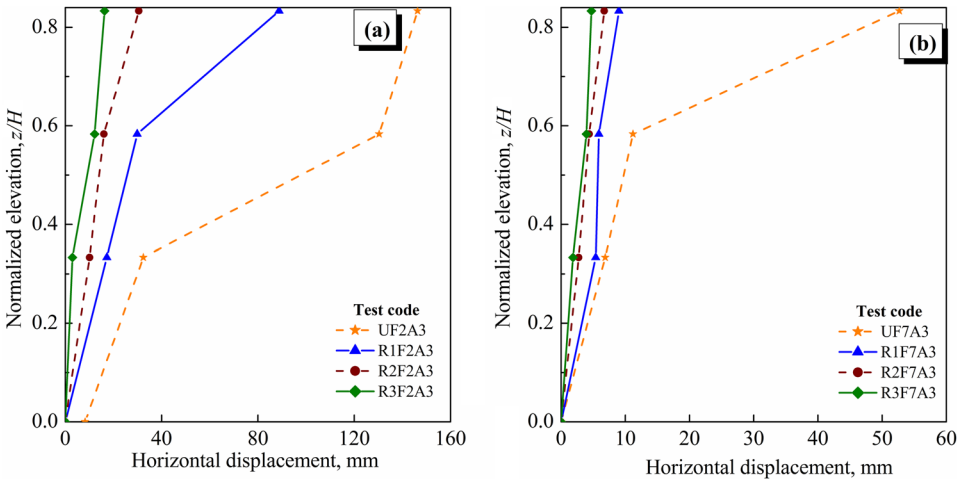

Fig. 12 Displacement response of unreinforced and different geogrid-reinforced slopes at different frequencies **a** 2 Hz and **b** 7 Hz

slopes is extensively improved with the reinforcement of slopes as the layers of reinforcement generate confinement effect which prevents the ease of transmission of vibrations through soil layers, which is unlikely in the case of unreinforced soils. Also, the effects are more pronounced for high frequency shaking because of increase in damping due to viscous energy losses, resulting in increase in interface friction between sand and reinforcement at higher frequencies. Some of the earlier researchers suggested that the dynamic interface friction angle does not depend on the frequency of shaking [53]. Though the effects of frequency on dynamic interface friction angle are not direct, at higher shaking frequencies, the soil in the slope gets densified, resulting in increased interface friction [54–56].

Seismic Deformation Analysis of Model Slopes

Results from the shaking table model studies carried out on unreinforced and reinforced soil slopes showed that the slopes have deformed due to base shaking and the deformations varied with the acceleration amplitude, frequency of shaking, and quantity of reinforcement in the slope. These deformations can be computed theoretically using analytical methods for comparison. Among the available procedures for seismic stability analysis of soil slopes, the sliding block method of Newmark [30] is extensively used by researchers since it is relatively simpler and reasonably accurate. Newmark's method computes the slope displacements using yield accelerations. Yield acceleration (k_y) is defined as the minimum pseudo-static acceleration that causes instability in the slope, which is analogous to the acceleration at which the factor of safety computed through limit equilibrium analysis becomes unity. Since the conventional Newmark's method uses a constant yield acceleration corresponding to the residual strength of the soil, slope deformations are over predicted.

Matasovic et al. [57] and Matasovic et al. [36] proposed a modified Newmark's rigid block analysis with degrading yield acceleration, which is particularly applicable to geosynthetic reinforced soils. This is a trilinear degradation model in which the yield acceleration (k_y) is highest ($k_{y(P)}$) initially, where the shear strength of the soil is assumed to be equal to the peak shear strength and it starts degrading linearly after a threshold displacement (δ_1) is reached and reaches a final residual value ($k_{y(R)}$) at the second threshold displacement (δ_2) corresponding to the residual shear strength of soil. In the present study, a similar analysis is used to compute the slope deformations. To obtain the deformations, accelerations falling above the yield acceleration in the acceleration time history are integrated twice. Yield accelerations corresponding to peak shear strength ($k_{y(P)}$) and yield acceleration corresponding to residual shear strength ($k_{y(R)}$) are computed separately and the integrations are carried out separately, to obtain two values for slope deformations, as shown in Fig. 13. The theoretical slope deformations are within the range of these two values.

Analysis showed that the unreinforced slopes are close to failure even under static conditions. Yield acceleration computed for unreinforced slopes is 0.061 g, which is much lower than the shaking accelerations used in the model tests. Hence, the deformations measured in unreinforced model slopes are very high. Slope deformations measured from the experiments are compared with the deformations obtained from the analytical studies. Since maximum deformations were observed at highest elevation, response accelerations of the model slopes measured through the accelerometers placed at highest elevation (A3) were used as input for the analysis. Time histories from the accelerometers were filtered through a lowpass FIR (finite impulse response) filter to remove noise in the signal, using a MATLAB program. The accelerations falling above the yield acceleration are then integrated to obtain relative velocity (v_{rel}), which is further integrated to obtain permanent deformations of the

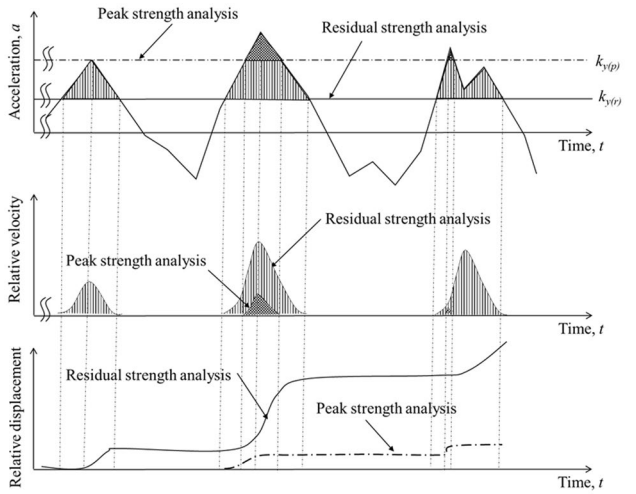

Fig. 13 Theoretical computation of permanent deformations from peak and residual yield accelerations

soil slopes (d_{rel}) during the period t_o to $t_o+\Delta t$ as per the following equations [45].

$$v_{\mathrm{rel}}(t) = \int_{t_o}^{t} a_{\mathrm{rel}}(t)dt = \left[A - k_y\right]\left(t - t_o\right), t_o \le t \le t_o + \Delta t \tag{2}$$

$$d_{\mathrm{rel}}(t) = \int_{t_o}^{t} v_{\mathrm{rel}}(t)dt = \left[A - k_y\right]\left(t - t_o\right)^2, t_o \le t \le t_o + \Delta t \tag{3}$$

In the above equations, A is the maximum response acceleration amplitude measured near the crest using the accelerometer A3 placed inside the model slope, t and t_o are corresponding time intervals, and k_y is the yield acceleration of the slope.

A numerical integration scheme was also developed using the MATLAB programming, in which the acceleration time history and yield acceleration were used as input to get velocity and displacement time histories directly. This exercise of computing permanent deformations in slope using Newmark's analysis is carried out for unreinforced and reinforced model slopes made of sand subjected to a shaking acceleration of 0.3 g and different frequencies, and the results are compared with the experimental measurements. The accuracy of the integration scheme was verified by computing the area under simple curves using the MATLAB algorithm and calculations done in an Excel spreadsheet. The algorithm gave exact values for these computations.

Figure 14 shows the computation of permanent deformations for the case of 45° unreinforced slope made of sand subjected to an acceleration of 0.3 g at a frequency of 2 Hz. Figure 14a shows the acceleration time history measured at highest elevation. The yield acceleration ($k_{y(P)}$) corresponding to peak shear strength is calculated as 0.061 g by equating the pseudo-static factor of safety to 1.0 using peak friction angle (φ_P) of 38°. Similarly, the yield acceleration ($k_{y(R)}$) corresponding to the residual shear strength of the soil is calculated as 0.044 g by equating the pseudo-static factor of safety to 1.0 using residual friction angle (φ_R) of 32°. These accelerations are marked on the acceleration time history plot obtained at A3, as shown in Fig. 14. Accelerations beyond the yield acceleration are responsible for permanent deformations in slope. These accelerations are double integrated within the time interval to obtain the permanent deformations of the slope, for both peak and residual cases. The velocity and displacement responses obtained by integrating the acceleration response beyond yield acceleration are shown in Fig. 14b, c, respectively.

Similar procedure was adopted for computing the deformations for the unreinforced slope at other frequencies and for reinforced slopes. Estimation of permanent deformations

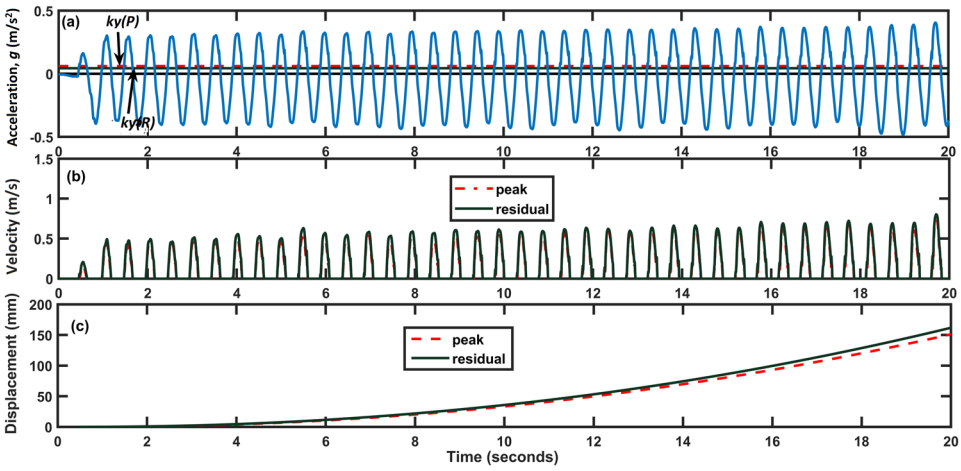

Fig. 14 Permanent deformations of unreinforced slope made of sand subjected to an acceleration of 0.3 g and frequency of 2 Hz

for unreinforced slope at 0.3 *g* acceleration and 7 Hz frequency is shown in Fig. 15.

To compute the peak and residual friction angles for geogrid-reinforced sand, shear strength improvement index proposed by Infante et al. [58] is used. Based on direct shear tests on sands of different gradation and relative density reinforced with different types of geosynthetics, Infante et al. [58] proposed improvement factors for peak and residual friction angles of reinforced sand. Well-graded sands and poorly graded sands at a loose state corresponding to 10% relative density and a dense state corresponding to 90% relative density, reinforced with uniaxial and biaxial geogrids were tested to determine the improvement in peak and residual friction angles. Geogrids were placed perpendicular to the shearing plane to determine the friction angles of reinforced sand, unlike the interface shear tests where reinforcement is placed along the shearing plane to determine the interface friction angle. In the present study, the relative density of sand in models is 55%. Shear strength improvement index for peak and residual friction angles for different sands at different relative densities, reinforced with different geosynthetics are measured and presented in tables by Infante et al. [58]. The shear strength improvement indices for peak and residual friction angles for the present sand reinforced with biaxial geogrid are taken as 1.23 and 1.08, respectively. These are the least possible improvement indices for poorly graded sand reinforced with a biaxial geogrid. The yield acceleration of reinforced model slopes ($k_{y(P)}$) corresponding to the peak shear strength is calculated as 0.146 *g* by equating the pseudo-static factor of safety to 1.0 using peak friction angle (φ_P) of 46.7°. Similarly, the yield acceleration of reinforced model slopes ($k_{y(R)}$) corresponding to the residual shear strength of the soil is calculated as 0.113 g by equating the pseudo-static factor of safety to 1.0 using residual friction angle (φ_R) of 41°. The factor of safety for the reinforced soil slope is computed as 1.55, considering the peak friction angle. Figure 16 shows the theoretical calculation of permanent deformations of single layer geogrid-reinforced slope at

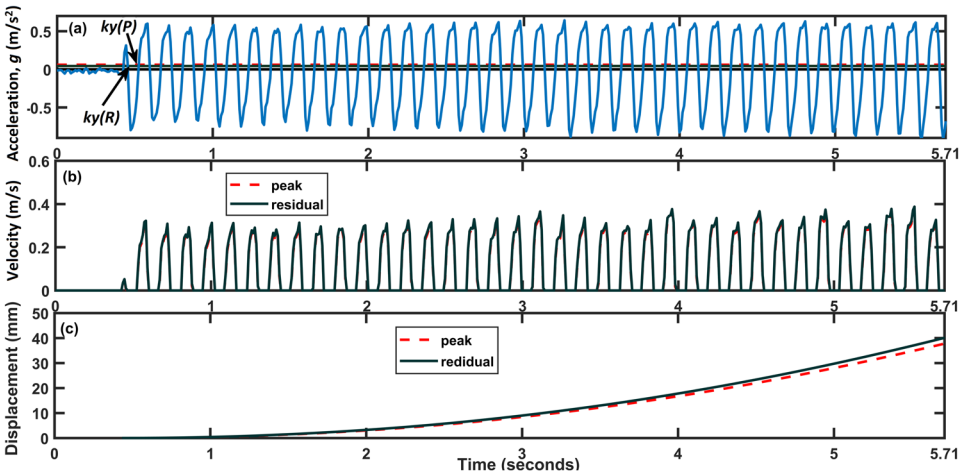

Fig. 15 Permanent deformations of unreinforced slope made of sand subjected to an acceleration of 0.3 g and frequency of 7 Hz

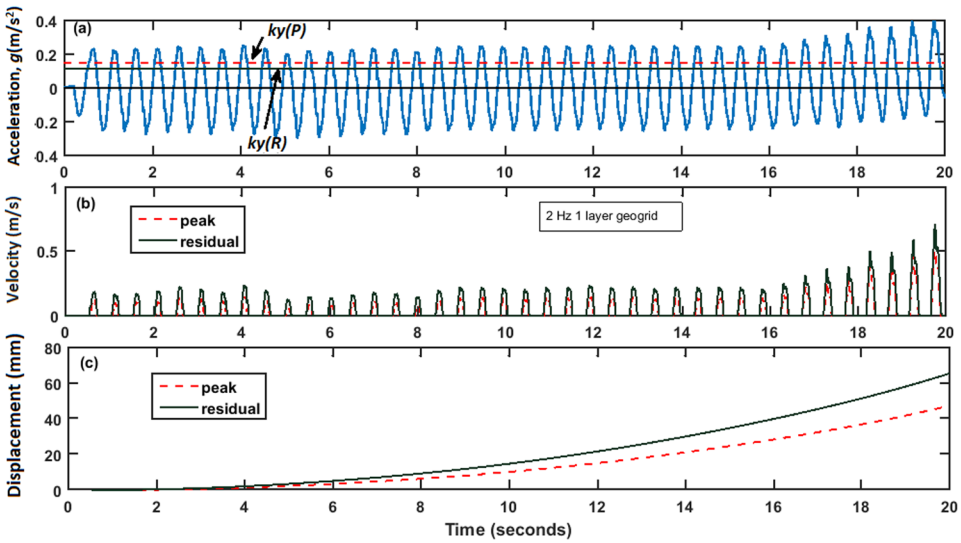

Fig. 16 Permanent deformations of one-layer geogrid-reinforced slope at 2 Hz frequency

2 Hz frequency. Estimation of permanent deformations for single layer geogrid-reinforced slopes at a frequency of 7 Hz is given in Fig. 17. Figures 18 and 19 show the calculation of permanent displacements for two-layer geogrid-reinforced slope at frequencies 2 Hz and 7 Hz, respectively. Similarly, Figs. 20 and 21 show the calculation of permanent displacements for three-layer geogrid-reinforced slope model at 2 Hz and 7 Hz frequencies, respectively.

The peak and residual friction angles and yield accelerations computed for different cases and the corresponding permanent deformations are shown in Table 4 along with the deformations measured from the model studies, for comparison. Comparison of predicted and measured displacements of unreinforced and various reinforced model slopes show that displacements measured in unreinforced model slopes at all frequencies are in reasonably good agreement with the estimated range of displacements, with less than 20% deviation from the theoretical range of deformations. However, in reinforced slope models, deformations measured at higher frequency of 7 Hz are not matching with the analytical predictions. However, the results are in reasonably good agreement at lower frequencies. Comparison of predicted and measured displacements of unreinforced model slopes at different time intervals at frequencies 2 Hz, 5 Hz, and 7 Hz are presented in Fig. 22. Acceleration amplitude in all these model tests was 0.3 *g*. Displacements predicted by theoretical analysis are in reasonably good agreement with measured displacements for unreinforced slope models at all frequencies. Comparison of predicted and measured displacements of one-layer, two-layer, and three-layer reinforced model slopes at different time intervals at frequencies 2 Hz and 7 Hz and an acceleration of 0.3 g are presented in Figs. 23, 24, and 25, respectively. In case of reinforced soil slopes, measured deformations are not matching well with the analytical predictions, the deviation increasing with the increase in frequency and with number of cycles. The effects of frequency of shaking on interface friction is the reason for the large difference in the predicted and measured

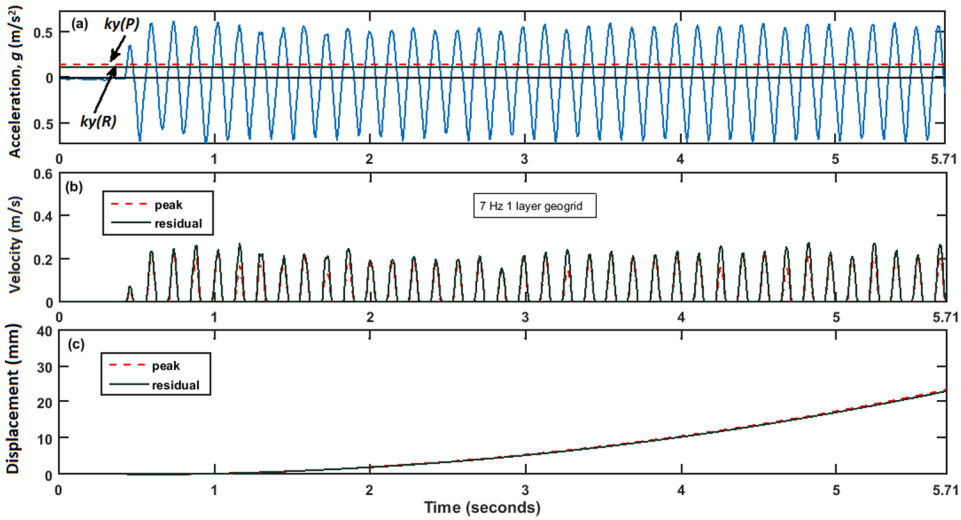

Fig. 17 Permanent deformations of one-layer geogrid-reinforced slope at 7 Hz frequency

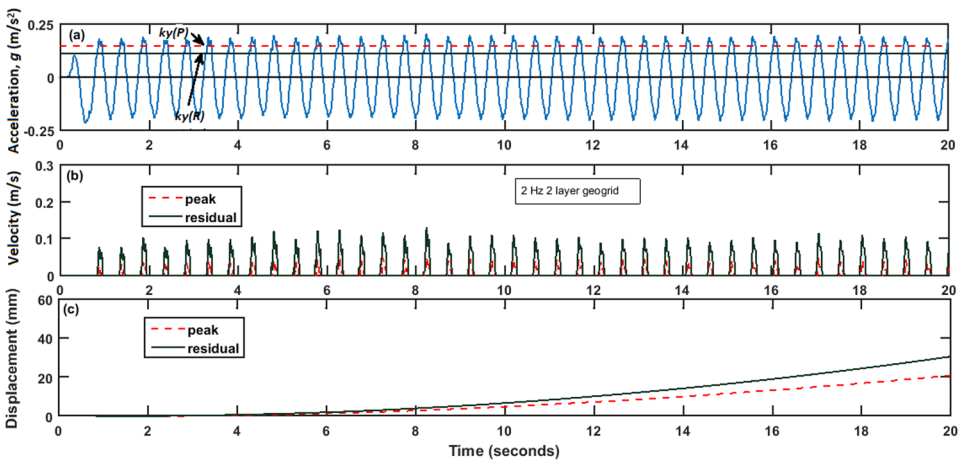

Fig. 18 Permanent deformations of two-layer geogrid-reinforced slope at 2 Hz frequency

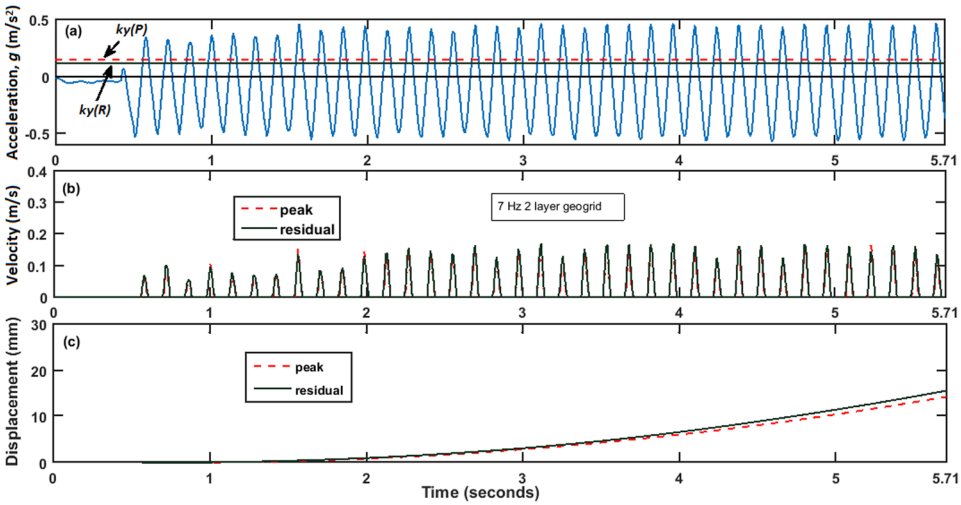

Fig. 19 Permanent deformations of two-layer geogrid-reinforced slope at 7 Hz frequency

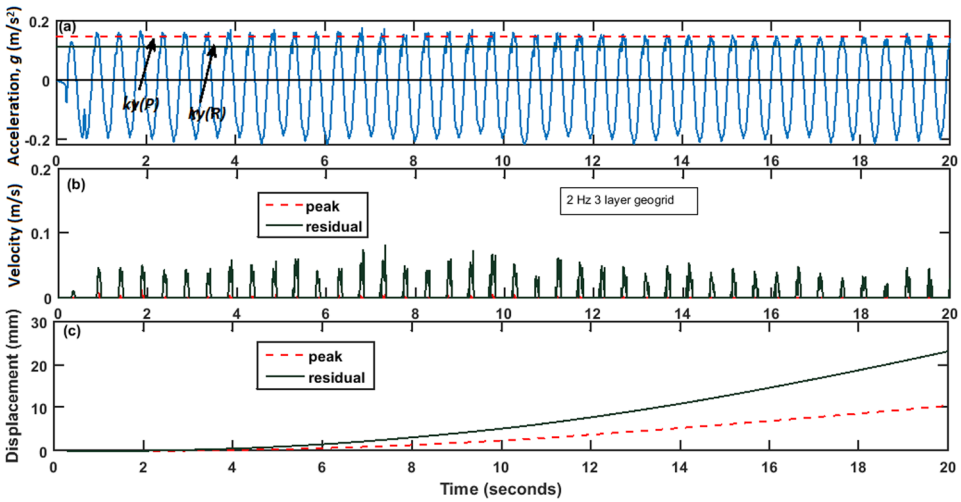

Fig. 20 Permanent deformations of three-layer geogrid-reinforced slope at 2 Hz frequency

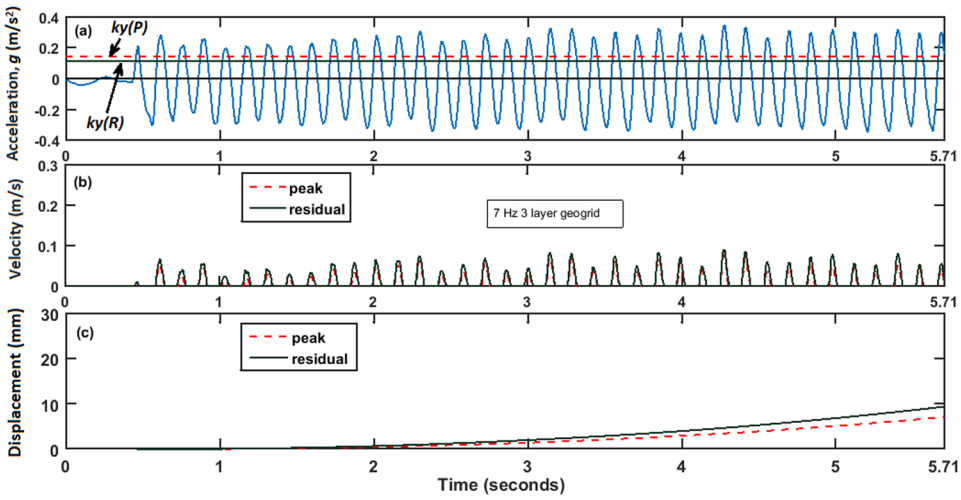

Fig. 21 Permanent deformations of three-layer geogrid-reinforced slope at 7 Hz frequency

Table 4 Comparison of predicted and measured displacements for different model slopes

Test code	Peak friction angle ϕ_P (degrees)	Residual friction angle ϕ_R (degrees)	Yield acceleration coefficient for ϕ_P $(k_{y(P)})$	Yield acceleration coefficient for ϕ_R $(k_{y(R)})$	Calculated displacement using $k_{y(P)}$ (mm)	Calculated displacement using $k_{y(R)}$ (mm)	Measured displacement (mm)
UF2A3	37	32	0.061	0.044	152.60	163.40	146.35
UF5A3	37	32	0.061	0.044	75.98	80.10	87.25
UF7A3	37	32	0.061	0.044	38.30	40.70	52.68
R1F2A3	43	40.5	0.146	0.113	48.30	66.65	88.81
R2F2A3	43	40.5	0.146	0.113	20.89	30.60	30.57
R3F2A3	43	40.5	0.146	0.113	10.54	23.12	16.33
R1F7A3	43	40.5	0.146	0.113	23.50	23.83	9.01
R2F7A3	43	40.5	0.146	0.113	14.28	15.10	6.74
R3F7A3	43	40.5	0.146	0.113	7.15	9.40	4.71

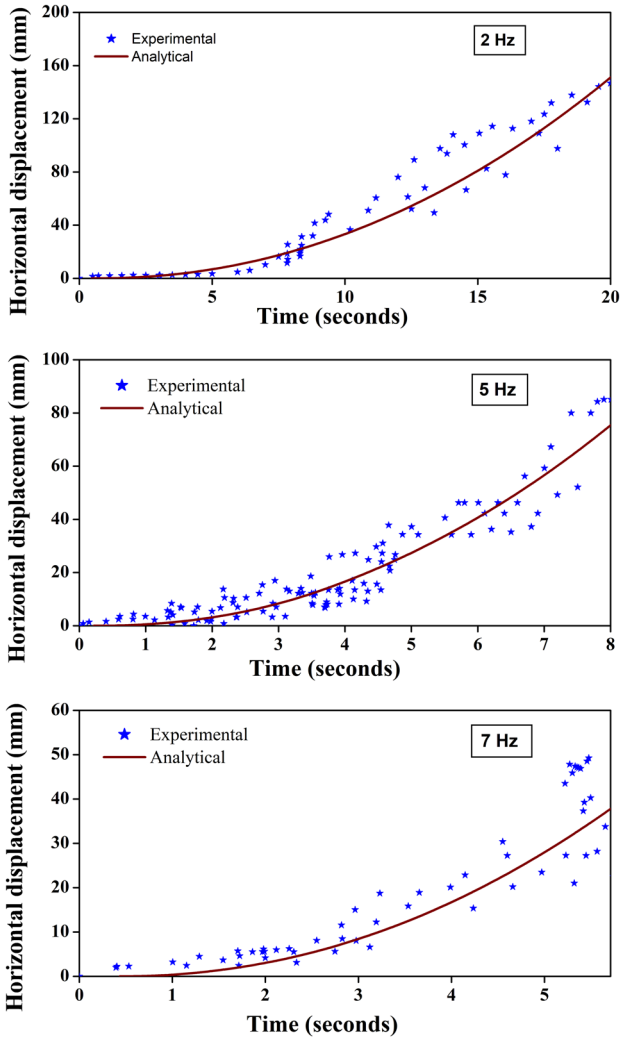

Fig. 22 Comparison of measured and permanent displacements of unreinforced model slopes at different frequencies

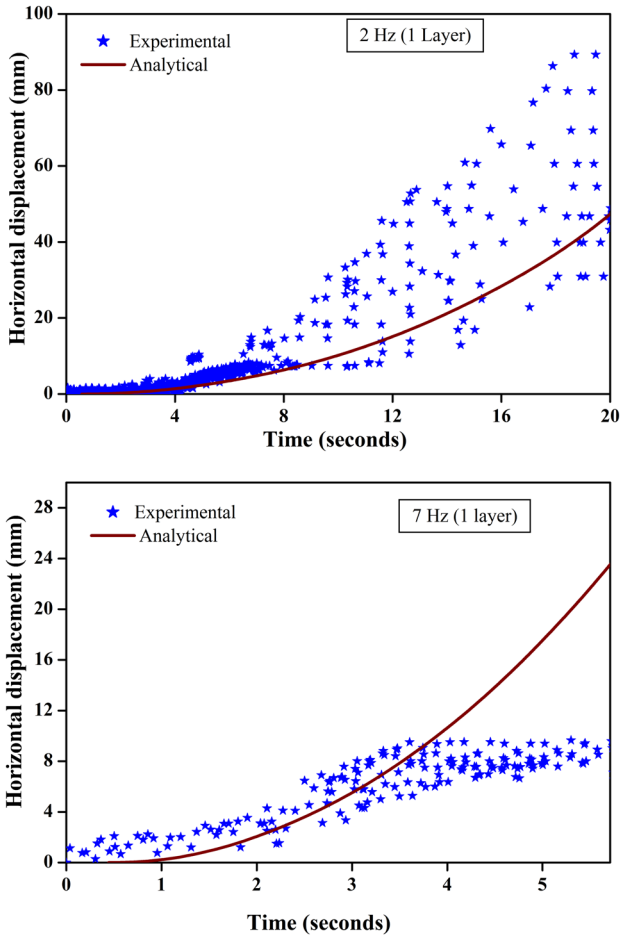

Fig. 23 Comparison of measured and permanent displacements of one-layer geogrid-reinforced model slopes at frequencies 2 Hz and 7 Hz

deformations at higher frequencies. Since Newmark's analysis assumes a rigid block displacement and the slope displacements in the present study are mostly rotational, there

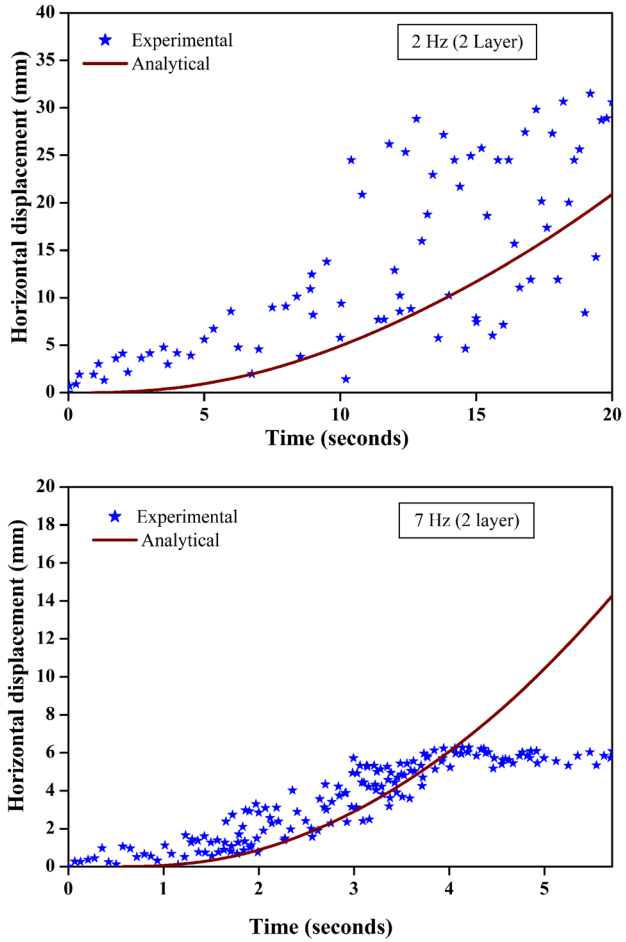

Fig. 24 Comparison of measured and permanent displacements of two-layer geogrid-reinforced model slopes at frequencies 2 Hz and 7 Hz

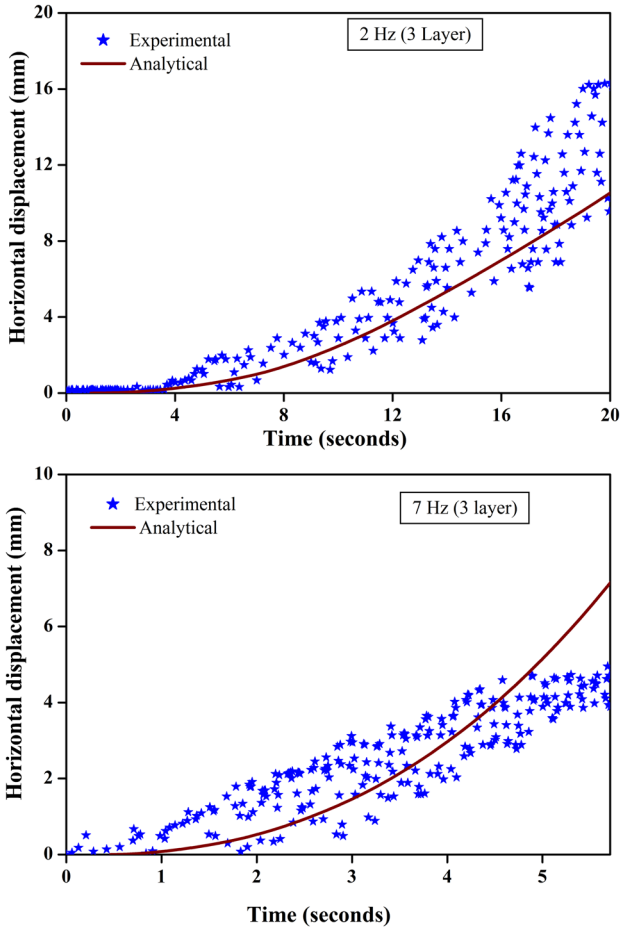

Fig. 25 Comparison of measured and permanent displacements of three-layer geogrid-reinforced model slopes at frequencies 2 Hz and 7 Hz

is significant mismatch between the measured and computed displacements, particularly when the frequency of shaking is high. Since the frequencies of most of the seismic events are around 1–2 Hz, the theoretical predictions can be used for predicting approximate slope deformations during a specific seismic event.

Shaking table studies are 1-*g* model tests and results obtained in this study have limitations of scaling effects. Laminar box used in the tests has minimal boundary effects. Since the subject of study is not level ground, the boundaries can affect the response of slope models to certain extent. Since these factors equally affect all slope models, the comparative response of unreinforced and reinforced models and effects of frequency and acceleration of shaking on the slope response outlined from this study are still valid. The increasing or decreasing trends of deformations and acceleration amplifications of the slopes with change in ground motion parameters are applicable only to the range of ground motion parameters, especially the excitation frequencies used in the present study. Appropriate similitude laws must be considered while applying the results to field size slopes.

Summary and Conclusions

Following major conclusions are drawn from the series of shaking table tests carried out on sand slope models and subsequent deformation analysis using modified Newmark's method.

- Sand slopes failed at low frequencies of shaking and remained intact at higher frequencies. Failure was sudden and catastrophic, resembling flow slide in slopes with a lot of cracks appearing on the slope face. Absence of fines in the soil led to the increase in pore connectivity in slopes and the pores got disconnected easily at lower frequencies, leading to higher slope deformations. At higher frequen-

cies, increased damping, and attenuation of seismic energy in sands reduced the slope deformations.

- The unreinforced slope displaced laterally by a maximum of 185.97 mm at 1 Hz frequency and the lateral displacement was reduced to 146.35 mm, 87.25 mm, and 52.68 mm for 2 Hz, 5 Hz, and 7 Hz frequencies, respectively.
- Unlike displacements, acceleration amplifications increased with increasing frequency. Maximum acceleration amplification factors were 1.02, 1.07, 1.25, and 2.13 for frequencies of 1, 2, 5, and 7 Hz, respectively.
- Increased base acceleration at a constant frequency of 2 Hz resulted in increased displacements. Maximum lateral displacement was measured as 3.34 mm at 0.1 *g*, 4.66 mm at 0.2 *g*, and 146.35 mm with a landslide mass behavior at 0.3 *g*.
- Effect of base acceleration on acceleration amplification factors is not significant for the small-scale models used in the present study.
- Geogrid reinforcement was effective in reducing the large deformations of slopes to a great extent. At 7 Hz frequency, maximum deformation in unreinforced model slope was 52.68 mm and the deformation reduced to 9.01 mm, 6.74 mm, and 4.71 mm respectively, for one, two, and three-layer geogrid-reinforced slopes subjected to similar base shaking. Maximum reduction in lateral deformations was about 88%.
- Permanent deformations of the model slopes computed using the modified Newmark's rigid block analysis for unreinforced and reinforced model slopes are compared with the maximum deformations measured in corresponding model slopes. Results showed that the measured deformations are in reasonably good agreement with the analytical computations for unreinforced cases at all frequencies and for reinforced cases at lower frequencies.
- Exact match of experimental and numerical deformations is not possible due to overall impact of the simplifying assumptions made in the Newmark's rigid block analysis and the limitations of 1-g model testing adopted in this study.

Acknowledgements Authors gratefully acknowledge the financial support through FIST grants of the Department of Science and Technology (DST), India, which was used for procuring the controller for the shaking table and the sensors used in the present study.

Data Availability The datasets generated during and/or analyzed during the current study are available from the corresponding author on reasonable request.

References

1. Jewell R (1980) Some effects of reinforcement on the mechanical behaviour of soils. PhD Thesis, University of Cambridge, London, UK
2. Jewell R, Wroth C (1987) Direct shear tests on reinforced sand. Geotechnique 37(1):53–68
3. Bathurst RJ, Cai Z (1995) Pseudo-static seismic analysis of geosynthetic reinforced segmental retaining walls. Geosynth Int 2(5):787–830
4. Sandri D (1994) Retaining walls stand up to the Northridge earthquake. Geotech Fabrics Rep 12(4):30–31
5. Sandri D (1997) A performance summary of reinforced soil structures in the greater Los Angeles area after the Northridge earthquake. Geotext Geomembr 15(4–6):235–253
6. Koga Y, Matsuo O (1990) Shaking table tests of embankment resting on liquefiable sandy ground. Soils Found 30(4):162–174
7. Bathurst RJ, Hatami K, Alfaro MC (2002) Geosynthetic reinforced soil walls and slopes: Seismic aspects. In: Geosynthetics and Their Applications, SK Shukla (Ed). Thomas Telford, London, 14, 327–392
8. El-Emam MM, Bathurst RJ (2007) Influence of reinforcement parameters on the seismic response of reduced-scale reinforced soil retaining walls. Geotext Geomembr 25(1):33–49
9. Lo Grasso AS, Maugeri M, Recalcati P (2005) Seismic behaviour of geosynthetic reinforced slopes with overload by shaking table tests. In: Slopes and Retaining structures under static and seismic conditions Gabr EA, Bowders JJ, Elton D, Zornberg JG, ASCE, GSP140, 1–14
10. Lin ML, Wang KL (2006) Seismic slope behaviour in a large-scale shaking table model test. Eng Geol 86(2):118–133
11. Varghese RM, Latha GM (2014) Shaking table studies on the conditions of sand liquefaction. In: Geo-Congress: Geo-characterization and Modeling for Sustainability 2014: 1244–1253
12. Latha GM, Varman AMN (2014) Shaking table studies on geosynthetic reinforced soil slopes. Int J Geotech Eng 8(3):299–306
13. Xu P, Hatami K, Jiang G (2020) Study on seismic stability and performance of reinforced soil walls using shaking table tests. Geotext Geomembr 48(1):82–97
14. Panah A, Eftekhari Z (2021) Shaking table tests on polymeric-strip reinforced-soil walls adjacent to a rock slope. Geotext Geomembr 49:737–756
15. Wolfe WE, Ranbir SS, Chohan HS (1988) The liquefaction potential of large scale sand samples subjected to irregular loading. In: Proc of 9th World Conference on Earthquake Engineering, Tokyo-Kyoto, Japan. 3, 303–308
16. Wood DM, Crewe A, Taylor C (2002) Shaking table testing of geotechnical models. Int J Phys Model Geotech 2(1):1–13
17. Clough RW, Pirtz D (1956) Earthquake resistance of rock-fill dams. Trans Am Soc Civ Eng 123(1):792–810
18. Iai S (1989) Similitude for shaking table tests on soil-structure-fluid models in 1g gravitational field. Soils Found 29(1):105–118
19. Telekes G, Sugimoto M, Agawa S (1994) Shaking table tests on reinforced embankment models. In: Proc of the 13th international conference on Soil Mechanics and Foundation Eng, pp 649–654
20. Sugimoto M, Ogawa S, Moriyama M (1994) Dynamic characteristics of reinforced embankments with steep slope by shaking model tests. In: Tatsuoka F, Leshchinsky D (eds) Recent case histories of permanent geosynthetic-reinforced soil walls. Proceedings of the Seiken Symposium, Tokyo, pp 271–275
21. Srilatha N, Latha GM, Puttappa CG (2016) Seismic response of soil slopes in shaking table tests: effect of type and quantity of reinforcement. Int J Geosynth Ground Eng. https://doi.org/10.1007/s40891-016-0074-2

22. Fahliani HK, Arvin MR, Hataf N (2021) Experimental model studies on strip footings resting on geocell-reinforced sand slopes. Int J Geosynth Ground Eng 7(2):1–15. https://doi.org/10.1007/s40891-021-00270-1
23. Matsuo O, Yokoyama K, Saito Y (1998) Shaking table tests and analyses of geosynthetic-reinforced soil retaining walls. Geosynth Int 5(1–2):97–126
24. Nova-Roessig L, Sitar N (2006) Centrifuge model studies of the seismic response of reinforced soil slopes. J Geotech Geoenviron Eng 132(3):388–400
25. Andersen EO (1997) A centrifuge modeling study of the seismic response of geosynthetic reinforced slopes, Doctoral dissertation, University of Washington, USA
26. Zornberg JG, Sitar N, Mitchell JK (1998) Performance of geosynthetic reinforced slopes at failure. J Geotech Geoenviron Eng 124(8):670–683
27. Brennan A, Madabhushi S (2009) Amplification of seismic accelerations at slope crests. Can Geotech J 46(5):585–594
28. Yu YZ, Deng LJ, Sun X, Lü H (2010) Centrifuge modeling of dynamic behavior of pile-reinforced slopes during earthquakes. J Central South Univ Technol 17(5):1070–1078
29. Yang KH, Hung WY, Kencana EY (2013) Acceleration-amplified responses of geosynthetic-reinforced soil structures with a wide range of input ground accelerations. In: Proc of Geo-Congress: Stability and Performance of Slopes and Embankments III, ASCE,1178–1187
30. Newmark NM (1965) Effect of earthquakes on dams and embankment The Rankine lecture. Geotechnique 15(2):139–160
31. Steedman RS, Zeng X (1990) The influence of phase on the calculation of pseudo-static earth pressure on a retaining wall. Geotechnique 40(1):103–112
32. Zeng X, Steedman RS (1993) On the behaviour of quay walls in earthquakes. Geotechnique 43(3):417–431
33. Choudhury D, Nimbalkar SS (2006) Pseudo-dynamic approach of seismic active earth pressure behind retaining wall. Geotech Geol Eng 24(5):1103–1113
34. Qin CB, Chian SC (2017) Kinematic stability of a two-stage slope in layered soils. Int J Geomech 17(9):06017006
35. Wartman J, Seed RB, Bray JD (2005) Shaking table modeling of seismically induced deformations in slopes. J Geotech Geoenviron Eng 131(5):610–622
36. Matasovic N, Kavazanjian E Jr, Giroud JP (1998) Newmark seismic deformation analysis for geosynthetic covers. Geosynth Int 5(1–2):237–264
37. Ichii K, Ohmi H (2004) Slope stability of cohesionless material under large seismic shakings. Proc of the 11th international conference on soil dynamics and earthquake engineering and the 3rd international conference on earthquake geotechnical engineering. University of California, Berkeley, pp 388–395
38. Wang KL, Lin ML (2011) Initiation and displacement of landslide induced by earthquake—a study of shaking table model slope test. Eng Geol 122(1):106–114
39. Kawai T (2005) Earthquake—scale modeling in the geotechnical engineering field. In: Saito K, Ito A, Nakamura Y, Kuwana K (eds) Progress in scale modeling, vol II. Springer, Cham, pp 21–43
40. Zhang Z, Fleurisson J, Pellet F (2018) The effects of slope topography on acceleration amplification and interaction between slope topography and seismic input motion. Soil Dyn Earthq Eng 113:420–431
41. Krishna AM, Latha GM (2009) Container boundary effects in shaking table tests on reinforced soil wall models. Int J Phys Model Geotech ICE Publishing 9(4):1–14
42. ASTM D6637 / D6637M-15 (2015) Standard Test Method for Determining Tensile Properties of Geogrids by the Single or Multi-Rib Tensile Method, ASTM International, West Conshohocken, Pennsylvania, USA
43. IS: 2720 (part 11) -1993. Methods of test for soils: Determination of shear strength parameters of a specimen tested in unconsolidated undrained triaxial compression without the measurement of pore water pressure. Bureau of Indian Standards, New Delhi
44. Dobie M (2011) Internal stability of reinforced soil structures using a two-part wedge method. In: 9th Indonesian Geotechnical Conference and 15th Annual Scientific Meeting, Jakarta, pp 61–72
45. Kramer SL (2004) Geotechnical earthquake engineering. Prentice Hall, Upper Saddle River, p 653
46. Lo Grasso AS, Maugeri M, Montanilli F, Recalcati P (2004) Response of geosynthetic reinforced soil wall under seismic condition by shaking table tests. In: Proc of 3rd European Geosynthetics Conference, Munich, Germany 1–3 March (2),723–728
47. Goldman S (1999) Vibration spectrum analysis: a practical approach, 2nd edn. Industrial Press, New York
48. Wood CW (2018) Resonance revealed: understanding what really happens at resonance. Vibrations 35(1):4–10
49. Quan Y, Harris JM (1997) Seismic attenuation tomography using the frequency shift method. Geophysics 62(3):895–905
50. Evans SG, Bent AL (2004) The Las Colinas landslide, Santa Tecla: a highly destructive flowslide triggered by the January 13. El Salvador earthquake Special Papers Geol Soc Am 2001:25–38
51. Lihua L, Zengle R, Guangxin L, Henglin X, Zhiyong Y, Chao Y, Feilong C (2017) Shaking table model tests for composite reinforced slopes. J Southwest Jiaotong Univ 52(3):496–504
52. Huang CC, Horng JC, Charng JJ (2008) Seismic stability of reinforced slopes: failure mechanisms and displacements. Geosynth Int 15(5):333–349
53. Yegian MK, Lahlaf AM (1992) Dynamic interface shear strength properties of geomembranes and geotextiles. J Geotech Eng ASCE 118(5):760–779
54. Linger DA (1963) Effect of vibration on soil properties. Highway Research Record 22
55. Park IJ, Seo MW, Park JB, Kwon SY, Lee JS (2004) Estimation of the dynamic properties for geosynthetic interfaces. In: Proc of 13th World Conference on Earthquake Eng, Vancouver, B.C, Canada, 1–6: Paper No. 3210
56. O'Rourke TD, Drusche SJ, Netravali AN (1990) Shear strength characteristics of sand-polymer interfaces. J Geotech Eng 116(3):451–469
57. Matasovic NJr, Kavazanjian E (1997) Newmark deformation analysis with degrading yield acceleration. In: Proc of Geosynthetics'97, Long Beach, CA, USA, 2, 989–1000
58. Infante DJU, Martinez GMA, Arrua PA, Eberhardt M (2016) Shear strength behavior of different geosynthetic reinforced soil structure from direct shear test. Int J Geosynth Ground Eng 2(17):1–16